CPP

Contributions to Plasma Physics

WILEY-VCH

REPRINT

Controlled Levitation of Dust Particles in RF+DC Discharges

N. Kh. Bastykova[1][*], **A. Zs. Kovács**[2], **I. Korolov**[2], **S. K. Kodanova**[1], **T. S. Ramazanov**[1], **P. Hartmann**[2], and **Z. Donkó**[2]

[1] IETP, Al-Farabi Kazakh National University, 71 Al-Farabi av., Almaty 050040, Kazakhstan

[2] Institute for Solid State Physics and Optics, Wigner Research Centre for Physics, Hungarian Academy of Sciences, 1525 Budapest, POB. 49, Hungary

Experiments and particle-based kinetic simulations were performed to obtain the equilibrium levitation height of dust particles in plane parallel electrode discharges in low pressure argon gas, established by combined RF and DC excitation. The computed values were compared to experimental data. The good overall agreement of the simulation results and the experimental data verifies our gas discharge, dust charging, as well as dust force balance models.

1 Introduction

Layers of dust particles are routinely generated in low-pressure gas discharges and many of their properties (structure, phase transitions, collective excitations, and transport properties) have thoroughly been investigated. For a range of conditions (properties of the dust particles and characteristics of the discharge plasma) a single layer of dust particles can be levitated, the position of which is defined by the balance of the forces acting on the particles. This position can be tuned by changing the characteristics of the plasma that surrounds the particles and serves as a source of charging of the dust [1–4]. The position of the dust layer can easily be determined experimentally by side-on observation of the system. Parallel to experiments, theoretical models of the dust charging, combined with a discharge model, make it possible to calculate the levitation height. Our aim is here to examine the validity of such a model via measuring and calculating the position of a dust layer in a radio frequency (RF) discharge in the presence of an additional DC bias that allows manipulation of the equilibrium position.

2 Experiment

In our experiments two flat stainless steel electrodes with a diameter of $D = 170$ mm are placed horizontally, at an adjustable distance of $L = 25 \ldots 36$ mm from each other, inside a glass cylinder, as shown in Figure 1. The lower electrode is powered via a coaxial feedthrough by an RF power supply operating at $f_{\mathrm{RF}} = 13.56$ MHz. We apply a peak-to-peak voltage between $V_{\mathrm{pp}} = 90$ V $\ldots 150$ V. The argon pressure is set at values of $p = 5.6$ Pa, 10 Pa, and 20 Pa, at a gas flow of approx. 0.1 sccm. A separate power supply, connected to the powered electrode via a RF choke makes it possible to introduce an *external* DC bias between -100 V and $+100$ V. We note that due to the high degree of symmetry of the electrode configuration the DC *self bias* of the plasma is below 2 V.

Melamine-formaldehyde (MF) spherical micro-particles with a radius of $r_{\mathrm{d}} = 2.19 \ \mu$m are dropped into the discharge plasma through a small opening in the centre of the upper, grounded electrode. This opening is covered with a 400 lines per inch stainless steel mesh, to confine the plasma between the electrodes and to provide a proper boundary condition for the modeling studies. The particle cloud is illuminated through a side window with a vertical light sheet from a 440 nm wavelength laser source. We use an Allied Version Prosilica CCD camera, equipped with a 50 mm focal length photographic lens to image the light scattered from the dust

---

[*] Corresponding author. E-mail: bastykova_nuriya@physics.kz

particles. The levitation height is determined from the recorded images after performing a pixel to mm length calibration.

To reach conditions for reproducible measurements the system is pumped a few days and 10-minutes "cleaning" DC discharges are used preceding the experiments, with both positive and negative voltages applied to the lower electrode, at $\approx$ 7 mA current. These DC discharges serve to pre-condition the stainless steel electrodes by sputtering. This preparatory procedure and the capability to reach a low base pressure of the system, about 2×10^{-6} mbar, provides the necessary cleanliness for reproducibility.
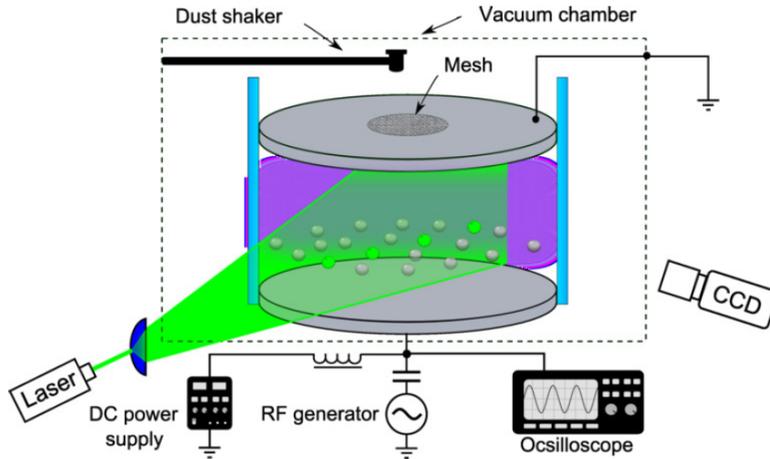

Fig. 1 Scheme of the experimental setup.

3 PIC/MCC simulation

The discharge is described by Particle-in-Cell simulation incorporating Monte Carlo treatment of collision processes (PIC/MCC) [5–8]. The code considers one spatial dimension and traces about 2×10^5 superparticles, representing electrons and argon ions. We assume that the density of the dust is low, i.e. the presence of the dust has no influence on the discharge characteristics. This approach, although it breaks the complete self-consistency, avoids the problems that arise because of the extremely different timescales of the motion of electrons, ions, and the dust particles [9, 10]. For the interactions of charged particles with electrode surfaces we account for secondary electron emission (with a secondary electron yield $\gamma = 0.08$) and the reflection of electrons (with probability of $\eta = 0.35$).

The main aim of our simulations is to determine the position x_d, where the dust layer settles in the discharge. We expect this position to be in the vicinity of the sheath/bulk boundary above the lower electrode of the discharge, at a position defined by the balance of the vertical forces acting on the particles (we neglect the dust-dust interaction, due to the low dust density, so only vertical forces are important). We consider the following three forces, which are expected to be important for the conditions of our studies: gravity, electrostatic, and ion drag forces.

- The force due to gravity is given as

$$F_g = m_d g, \tag{1}$$

where m_d is the mass of the dust particles.

- The electrostatic force is

$$F_{el} = < E(x) > q_d, \tag{2}$$

where $< E(x) >$ is the time-average of the electric field at position x (as obtained from the PIC/MCC simulation of the discharge without dust) and q_d is the dust charge. The calculation of this force needs

the determination of the charge of the dust particles, q_{d}. For that, the first step is to calculate the floating potential, φ_{d}. For the determination of φ_{d} we apply the method of [11], which is based on the interactions (collisions) between electrons and ions with the dust particles, described by cross sections that correspond to the Orbital Motion Limited (OML) approximation. We assume that a dust particle is located at each grid point (x_{k}) in the simulation and carry out calculations for the floating potential at all grid points. We emphasize that this is only needed to determine the forces as a function of x, and finally the real position of the dust layer will be determined by the balance of the three forces listed above. The calculation of the floating potential, φ_{d}, proceeds in the following way: we run the PIC/MCC simulation for one RF cycle, and meanwhile calculate the electron and ion fluxes to dust particles (Γ_{e} and Γ_{i}), by summing for all electrons and ions, respectively:

$$\Gamma_{\mathrm{e}} \propto \sum_p W_{\mathrm{e}} v_p \sigma_{\mathrm{ed}}[\varepsilon_p, \varphi_{\mathrm{d}}(x_{\mathrm{k}})] \tag{3}$$

$$\Gamma_{\mathrm{i}} \propto \sum_p W_{\mathrm{i}} v_p \sigma_{\mathrm{id}}[\varepsilon_p, \varphi_{\mathrm{d}}(x_{\mathrm{k}})] \tag{4}$$

where W denotes the superparticle weight, v_p is the velocity of the p-th electron or ion, σ_{ed} and σ_{id} are the electron-dust and ion-dust collision (collection) cross sections [12]. The floating potential of the dust particles is found iteratively, by the requirement that (3) and (4) become equal in the stationary state, at all positions. $\varphi_{\mathrm{d}}(x_{\mathrm{k}})$ is changed by $\pm 0.05\mathrm{V}$ after each RF simulation cycle at each position to reach the above mentioned requirement. Having obtained $\varphi_{\mathrm{d}}(x_{\mathrm{k}})$ the equilibrium dust charge is found adopting the simple capacitor model according to which:

$$q_{\mathrm{d}} = 4\pi\varepsilon_0 r_{\mathrm{d}}\varphi_{\mathrm{d}}(x_{\mathrm{k}}). \tag{5}$$

From this known value of the charge we calculate the electrostatic force, with spatial dependence, $F_{\mathrm{el}}(x)$.

- Ion drag force. This force results from the momentum transfer from the ions flowing to the dust particles [13]. It consists of two parts: (i) ions absorbed by the dust particles, and (ii) ions deflected by the charged dust particles. The two corresponding force components are called the collection force and the orbit force:

$$F_{\mathrm{i}}(x) = F_{\mathrm{i,coll}}(x) + F_{\mathrm{i,orb}}(x). \tag{6}$$

The usual way to handle these processes is to adopt the binary collision model. We proceed with the calculation based on the model of [13]. The required data (drift and mean velocities of the ions) are readily available from the PIC/MCC simulation.

Finally the equilibrium position of the dust particles is derived from the force balance:

$$F_{\mathrm{tot}} = F_{\mathrm{el}}(x_{\mathrm{d}}) - F_{\mathrm{g}} - F_{\mathrm{i}}(x_{\mathrm{d}}) = 0. \tag{7}$$

4 Results

First we illustrate the general characteristics of the discharge plasma. Figure 2 shows the spatiotemporal distribution of the electron density, obtained from the PIC/MCC simulation, for $V_{\mathrm{pp}} = 150$ V, at $p = 10$ Pa. Besides the "base case" when the discharge is driven by a pure harmonic RF voltage waveform (Figure 2(b)), we also display simulation results for two cases, when a DC voltage ($\pm$ 90 V) is superimposed at the driven electrode (external DC bias). At zero bias the electron density peaks in the center of the discharge the length of the sheaths at both sides of the discharge are equal. Figure 2(b) reveals well the formation and collapse of the sheaths at both electrodes, at opposite phases of the excitation waveform. A superimposed negative DC bias shifts the peak of the density profile towards the grounded electrode and increases the length of the sheath at the negatively biased (powered) electrode, as shown in Figure 2(a). A positive bias results in the opposite behavior as it can be seen in Figure 2(c). The shift of the electron density peak is also accompanied by a decrease of the peak electron density in the cases of non-zero bias values.
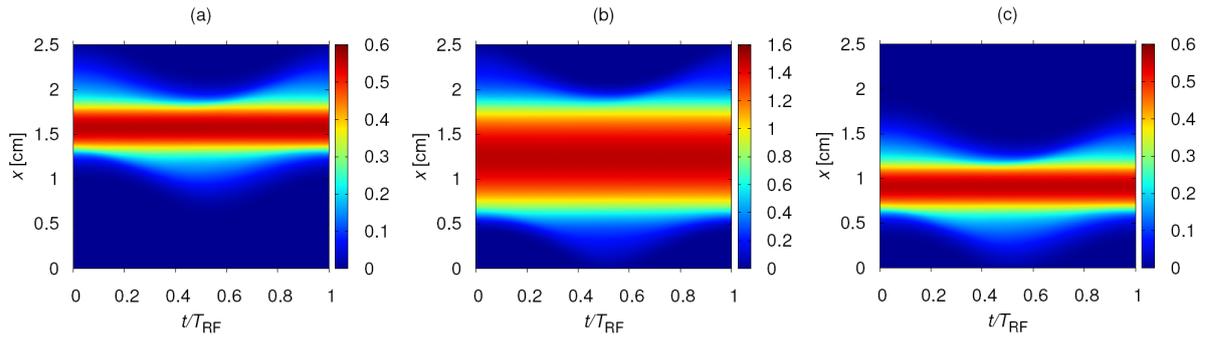
Fig. 2 Effect of DC bias on the spatio-temporal distribution of the electron density for $L = 25$ mm, $V_{pp} = 150$ V at $p = 10$ Pa with (a) $V_{DC} = -90$ V, (b) 0 V, and (c) 90 V. The color scales are given in unites of 10^9 cm^{-3}.

Next we illustrate (in Figure 3) the spatial dependence of the different force components described above, for conditions $V_{pp} = 150$ V, at $p = 10$ Pa, with $V_{DC} = 0$ V and $V_{DC} = -90$ V. The panels of the figures show only a part of the electrode gap, where the model is expected to be valid. (We note that the OML theory breaks down deep inside the sheath, leading to a non-physical solution.) Among the components of the ion drag force (6), the orbit force is found to be dominant, and the collision force is negligible. The equilibrium levitation position at $V_{DC} = 0$ V found as $F_{tot}(x_d) = 0$ is $x_d = 0.58$ cm. When a negative DC bias is applied to the plasma, the levitation height clearly increases as dictated by the increased sheath length at the powered electrode. The levitation position at $V_{DC} = -90$ V becomes $x_d = 1.26$ cm. The floating potential and the charge of the dust particles at the levitation height was found to be $\varphi_d \approx -7$ V, and $q_d \approx -10800$ e, respectively.
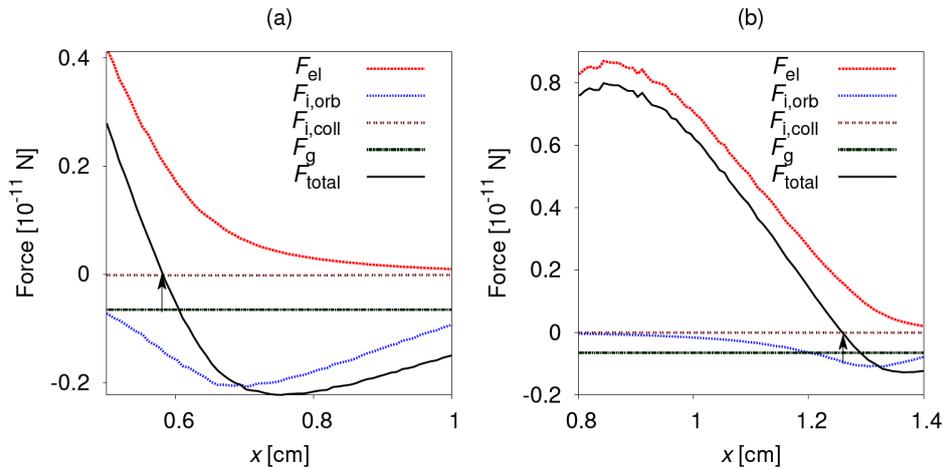

Fig. 3 Spatial dependence of the different force components, for conditions $L = 25$ mm, $V_{pp} = 150$ V at $p = 10$ Pa, $V_{DC} = 0$ V (a) and $V_{DC} = -90$ V (b).

In the experiment, as well as in the simulation the DC bias was scanned over a wide range, usually (except when more limited by the pressure and/or the gap size) within -100 V $\leq V_{DC} \leq 100$ V. The results of these scans, carried out at three different gas pressures, are given in Figure 4.

The curves recorded at different values of the pressure and electrode gap follow the same trend. At V_{DC}=0 V, at fixed gap length the levitation height (x_d) decreases with an increasing pressure, due to the decrease of the length of the sheaths. A longer electrode separation, at fixed pressure, results in slightly decreased x_d, again by the shorter sheaths that result from the higher peak densities at a greater L.

A negative DC bias voltage at the powered electrode results in an increase of the dust layer's levitation height in all cases and this position increases monotonically with the bias. This way, x_d can be tuned by a factor of 2 to 3, in absolute numbers, by up to 9 mm, in case of $p = 5.6$ Pa and $L = 36$ mm.

The positive DC bias values have marginal effect on x_{d}, as it can be seen in the panels of Figure 4.

We find a good general agreement between the experimental and calculated values of the levitation height for all sets of data obtained at the different gas pressures and gap length values. This agreement confirms that our discharge model and its implementation in the code, as well as the charging and force balance models adopted in the work describe the plasma + dust system considerably well, and that they are applicable for the range of conditions covered here. The observations, which have been explained by the discharge simulation results, confirm that the external DC bias provides a solid control over the position of the dust layer.
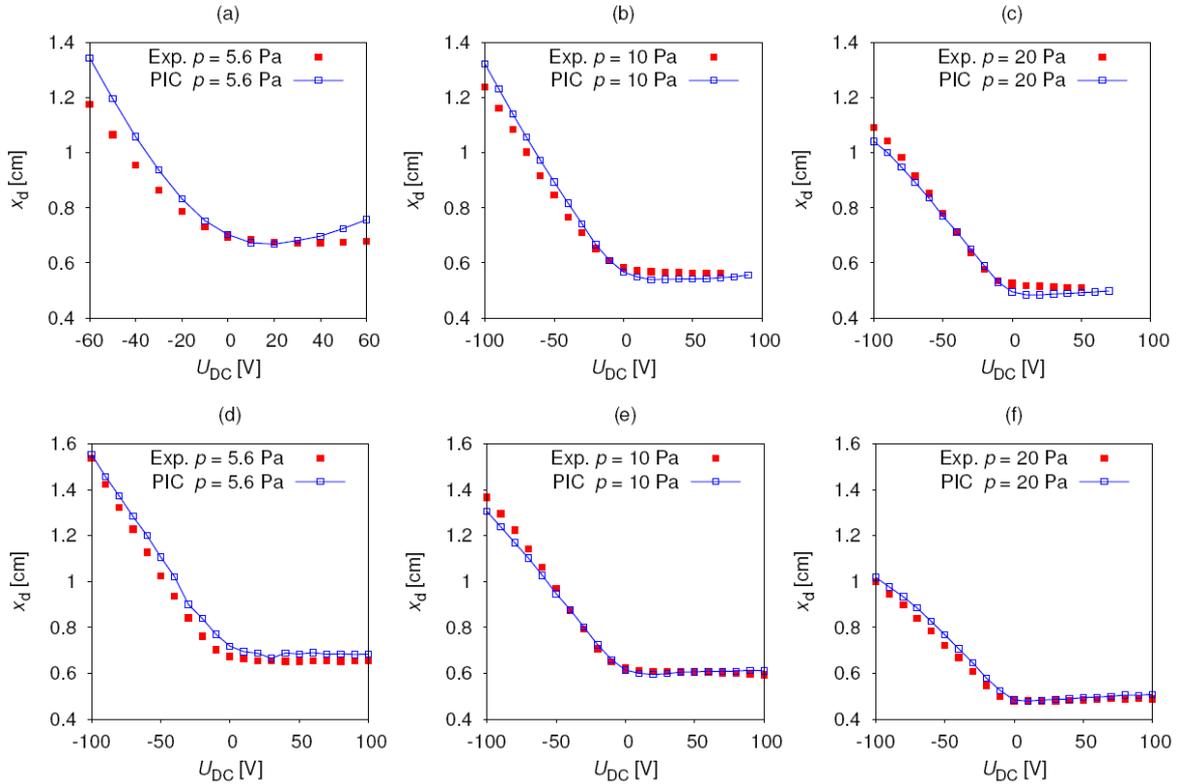
Fig. 4 Equilibrium position of the dust layer as a function of the DC bias, V_{DC}, for conditions: $V_{\mathrm{pp}} = 150$ V at $p = 5.6$ Pa, $p = 10$ Pa, $p = 20$ Pa, $L = 25$ mm (upper row) and $L = 36$ mm (lower row).

We note that the application of the OML theory imposes a upper limit on the buffer gas pressure, as it requires that (i) the ion mean free path is (much) longer than the Debye length and that (ii) the Debye length is also longer than the dust radius. Condition (ii) holds trivially. Our calculations show that the OML theory is near the limits of its applicability at 20 Pa. Therefore we have only showed results for the $p \leq 20$ Pa pressure range. (At the higher pressure of 40 Pa we have found significant differences between the experimental data and simulation results, which can indeed be attributed to the breakdown of the OML approximation). For the extension of the parameter range covered here the model has to be upgraded by including, e.g., more sophisticated calculations for the drag forces as given in [14] and more complete description of the dust charging [15].

References

[1] M. Klindworth, A. Melzer, A. Piel, and V.A. Schweigert, Phys. Rev. B **61**, 8404 (2000).
[2] V. Nosenko, J. Goree, and A. Piel, Phys. Plasmas **13**, 032106 (2006).

[3] V. Nosenko, A.V. Ivlev, and G.E. Morfill, Phys. Plasmas **17**, 123705 (2010).

[4] S. Iwashita , E. Schüngel, J. Schulze, P. Hartmann, Z. Donkó, G. Uchida, K. Koga, M. Shiratani, and U. Czarnetzki, J. Phys. D: Appl. Phys. **46**, 245202 (2013).

[5] C.K. Birdsall, IEEE Trans. Plasma Sci. **19**, 65 (1991).

[6] K. Matyash, R. Schneider, F. Taccogna, A. Hatayama, S. Longo, M. Capitelli, D. Tskhakaya, and F.X. Bronold, Contrib. Plasma Phys. **47**, 595 (2007).

[7] S. Longo, M. Capitelli, and K. Hassouni, J. Phys. IV France 07, C4-271 (1997).

[8] Z. Donkó, Plasma Sources Sci. Technol. **20**, 024001 (2011).

[9] K. Matyash, R. Schneider, and H. Kersten, J. Phys.: Conf. Series **11**, 248 (2005).

[10] V. Land, L.S. Matthews, T.W. Hyde, and D. Bolser, Phys. Rev. E **81**, 056402 (2010).

[11] A.L. Alexandrov, I.V. Schweigert, and F.M. Peeters, New J. Phys. **10**, 093025 (2008).

[12] S. A. Khrapak, A. V. Ivlev, Complex and Dusty Plasmas (CRC Press, eds. V. E. Fortov and G. E. Morfill) (2010).

[13] M.S. Barnes, J.H. Keller, J.C. Forster, J.A. O'Neill, and D.K. Coultas, Phys. Rev. Lett. **68**, 313 (1992).

[14] I.H. Hutchinson and C.B. Haakonsen, Phys. Plasmas **20**, 083701 (2013).

[15] W.J. Miloch, Journal of Plasma Physics **80**, 795 (2014).